Relativistic Electron Generation and Its Behaviors Relevant to Fast Ignition

K. A. Tanaka[1),2)], H. Habara[1),2)] R. Kodama[1)),2], K. Kondo[1),2)], G.R. Kumar[1),2),3)], A.L. Lei[1),2)], K. Mima[1)], Y. Sentoku[4)], T. Tanimoto[1),2)], and T. Yabuuchi[1) ,2)]

[1)]Institute of Laser Engineering, Osaka University,
2-6 Yamada-Oka, Suita, Osaka 565-0871 Japan
[2)]Graduate School of Engineering, Osaka University,
2-1 Yamada-Oka, Suita, Osaka 565-0871 Japan
[3)]Tata Institute of Fundamental Research,
Homi Bahbha Rd., Mumbai 400 004 India
[4)] Department of Physics, University of Nevada,
Reno, Nevada 89521-0042 U.S.A.

e-mail contact: katanaka@ile.osaka-u.ac.jp

Abstract Ultra-intense laser (UIL) has been used to create relativistic hot electrons in order to study the behaviors relevant to fast ignition. The electrons generated on an oblique UIL incidence shows their transport along the target surface consistent with strong B field responsible with the phenomena. Gold foam was used to enhance the production of hot electrons via. UIL irradiation on a target. Heating appears of gold foam to be 3 times stronger than a plane gold target.

1. Introduction

Ultra-intense laser (UIL) systems with a considerable energy are now available to study high energy density matter physics. Especially these lasers are suitable for the studies of fast ignition (FI), electron acceleration, and plasma photonics devices. One such successful example is fast ignition[1]. Here gold cone was used to guide a fast heating laser pulse in order to heat a highly compressed plasma core up to 1 keV. The experiment was successful to show the fast heating effect with injection of a PW 500 J laser pulse. 30 % coupling efficiency was indicated in the experiment from the heating laser to the core. Based on this high efficiency 10 kJ PW laser is now under construction to test even higher fast heating temperature up to several keV at the Inst. Laser Engineering. Important issues are to understand the physics of hot electron generation[2], its energy transport, and the behaviors of the electrons within the cone[3] in order to figure out the feasibility of the large scale fast ignition integral experiments.

There is a prediction using PIC simulation to invoke surface hot electrons bound by intense magnetic fields (>MGauss) along the cone surface, where the gold cone puts the configuration of oblique laser incidence onto the gold surface [4]. Experiments were conducted focusing on this critical physics issue with GM-II: a 30 TW laser system with a sub-pico second pulse width and energy up to 20 J at 1053 nm wavelength. Focused laser intensities were varied up to 3x 10^{18} W/cm^2. The spatial distribution of hot electrons is measured at an oblique laser irradiation 60 degrees onto a plane target with or without pre-formed plasmas on the surface in order to reveal the surface hot electron behaviors. The production of hot electrons was shown clearly along the target surface with the plasma at a laser intensity 3×10^{18} W/cm^2. These electrons are transported along target surface and then are detected with imaging plate for its spatial distribution information. The results were compared with a PIC simulation results, consistent with 30 MGauss B field at the

target wall created by both hot and cold returning electrons.
A foam cone-in-shell target design is considered aiming at increased hot electron production for the fast ignition. A thin low-density foam is placed to cover the inner tip of a gold cone inserted in a fuel shell. An intense laser is then focused on the foam to generate hot electrons for the fast ignition. This may enhance the laser energy deposition in the compressed fuel plasma. Element experiments presented here demonstrate enhanced hot electron production and increased laser energy coupling with foam coated targets in comparison with solid targets without increasing the electron temperature and beam divergence from planar solid targets with thin low-density foam coating on the front surface. This indicates that our proposed foam cone- in-shell target offers considerable improvements over the gold cone-in-shell target that has been successfully used for demonstrating the potential of FI.

2. Hot electron generation at oblique incidence of UIL

The experiment was performed using the GMII 30 TW laser system at Osaka University[5]. The 1μm intense laser light (20 J/600 fs) irradiated a 20 μm Al target with a shallow incident angle, typically 60^{o} from the normal. Preformed plasma can be created before arriving the main pulse using a separate beam line with a long pulse duration (1 J/300 ps). The timing of main pulse is fixed at the peak of long pulse through the experiment. The size of preformed plasma was observed using an optical probe beam with an optical interferometer.

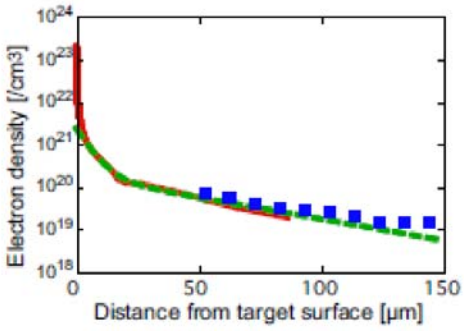

Figure 1. The electron density profiles (square:measured, line:1D and dotted line:2D simulations).

The solid squares in Fig. 1 show the experimental electron density gradient to the target normal direction. The solid line represents the calculated electron density which well agrees with the experimental result. As a convenience for further arguments, we obtain a good fitting curve covering the 2-D experimental data and the 1-D calculation result simultaneously using two 2 dimensional Maxwellians. The 2-D dashed line in Fig. 1 indicates the fitting curve to the normal which precisely reproduces both 1-D simulation and experimental curves. The emission angle of the fast electrons was measured with a stack of imaging plates (IP) (FUJI Film, BAS-SR2025), which is absolutely calibrated over a wide range of electron energies [6]. The stack consists of 4 IP layers and several filters including Al (12 μm), PET (500 μm), and Aclyle (5 mm x 3 layers between each IP layers) against ions and X-rays as well as ω_0 and $2\omega_0$ emissions. The stack was located 10 mm behind the target. To cover wide range of electron emission direction, the size of IP (H 63mm x W 38mm) is considerably larger than target size, 500 μm square. The signal position on IP is converted into angles to the target normal, i.e. the

vertical angle is taken for the tilting direction of the target. The electrons were clearly emitted to the laser axis and also outside of the specular direction when target was irradiated without any rear plasma. This outside specular emission is at the direction same as so called "secular jet" observed in the several previous experiments [7]. On the other hand, with the plasma condition, the electron emission shows remarkably changes according to laser intensity. Figure 2 (a), (b), and (c) indicates the emission direction taken at 1 x 10^{17}, 1 x 10^{18}, and 3 x 10^{18} W/cm^2 of laser intensity, respectively.

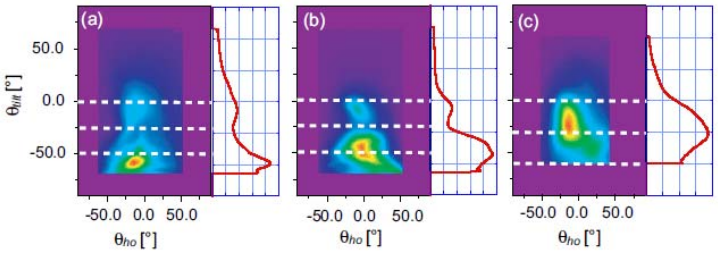

Figure 2 Intensity dependence of electron emission angle with plasma condition at (a) 1 x 10^{17}, (b)1 x 10^{18}, and (c) 3 x 10^{18} W/cm^2, respectively. The horizontal lines represent the laser axis, target surface, and specular directions from up to down. Due to a few % of target setting accuracy, the incident angles of each shot were (a) 66◦, (b) 64◦, and (c) 59◦.

In these figures, the three horizontal dashed lines represent the laser axis, target surface, and specular directions. Also the vertical line profile is added at the side of each image to identify the peak position easily. At the lower intensity, the emission direction is same as the direction without plasma case. However, as laser intensity increases, the emission becomes close to target surface direction. In particular, at highest intensity shot, the emission angle is completely on the target surface direction.
This surface electron acceleration mechanism has already explained by Sentoku and Nakamura [4]. At the critical surface, strong magnetic field is generated due to discontinuity of laser field according to Maxwell equation ($B(z) = \partial A(z)/\partial z$) at plasma surface. Then the fast electrons generated in laser plasma interactions are trapped by the magnetic field along the target surface. This surface current and its return current enhance the surface magnetic field. Such positive feedback holds the strong surface current during the laser irradiation. In order to confirm the possibility, we performed 2-dimensional PIC simulations with several laser and plasma conditions. Figure 3 shows the calculated 2-dimentional electron momentum distributions. The white rectangle represents initial plasma region and intense laser irradiates with 60◦ incident angle (arrow) on it. The two white dashed lines shows the laser incidence (right) and specular (left) directions. At near solid plasma condition (scale length L = 0.1 μm) with the laser intensity I = 10^{18} W/cm^2, the electron emission direction is strongly collimated toward the target surface direction, as well as a small fraction to laser direction as shown in Fig. 3 (a). However, when even a thin plasma exists (L = 0.5 μm), the electron acceleration directions are completely changed to a specular jet direction and almost no surface current can be observed (Fig. 3 (b)). On the other hand, when laser intensity increases to 10^{19} W/cm^2, the PIC calculation indicates the fast electron emission is recovered to the surface direction even the existence of small plasma (L = 0.5 μm) as shown in Fig. 3 (c).

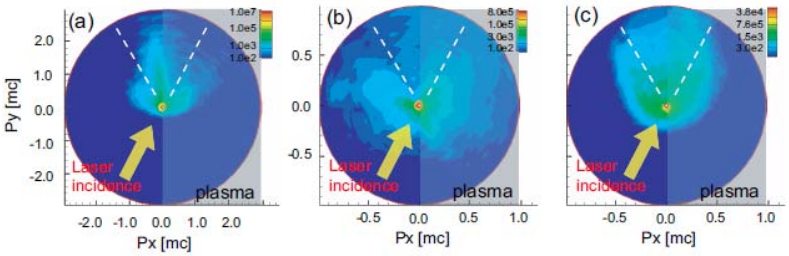

Figure 3 Electron momentum distribution changing laser intensity for (a) laser intensity $I = 10^{18}$ W/cm^2 and initial plasma scale length at critical $L = 0.1$ μm, (b) $I = 10^{18}$ W/cm^2 and $L = 0.5$ μm, and (c) $I = 10^{19}$ W/cm^2 and $L = 0.5$ μm. The plasma position is covered by gray box and laser incidence is represented by yellow allow in both figures.

These calculations strongly indicate that the sufficient strength of laser pressure is significantly important for surface static magnetic field which can create the surface current. The scale length dependence in the PIC calculations at the lower intensity case shows a contradiction to the experimental results. In addition, the electron emission to surface direction has observed experimentally even slightly lower intensity compared with the calculation. The emission cone angle of electrons to laser direction for no plasma case was clearly larger than that with plasma condition (<25◦ and >45◦ with and without plasma case). This fact, the reduction of electron emission cone angle, strongly suggests relativistic self-focusing in plasma [8,9] because the resulting higher intensity laser could transfer their moment onto the electrons more effectively. We have performed a 2-D ray-trace calculation to estimate the increase of laser intensity via relativistic self-focusing using a realistic plasma density taken from the interferometer images as above. At the start of the calculation, a Gaussian profile beam is located at 90 μm back from the target position, where the spot size become comparable to 20 μm in our focusing system, with 60 degrees incident angle in the simulation box. The calculation ends when the laser reaches at the relativistic critical density. As the result, at lower intensity case ($1x10^{18}$ W/cm^2) self-focusing does not almost occur because the power could be almost equivalent to the critical power of relativistic self-focusing ($P_c = 17.4(n_c/n_e)$ [GW]). On the other hand, at higher intensity case ($3\ x10^{18}$ W/cm^2), the laser intensity significantly increases to 10^{19} W/cm^2 as shown in table I. Such higher intensity laser light can reach 2 times of critical density due to relativistic transparency [10], where the scale length is almost 1 μm whereas the scale length at critical density is expected to be 3-4 μm from our plasma density. From these reasons, surface current formation is sufficiently possible at the high intensity case. It is possible to calculate the surface magnetic field from the bending angle of fast electrons. Assuming a Maxwellian as an electron energy distribution, the electron temperature is obtained from the least square fitting using the signal peak intensities and the average electron energy for each layer, resulting in 1.49 MeV at higher intensity case. Using this average energies, the strength of magnetic field is about 3.3 ($\pm$ 7%) MGauss / z [μm],

where z represents the depth of surface magnetic field. Assuming a skin depth (~100 nm) as the depth from the PIC result, the magnetic field becomes about 33 MGauss. This is about 12% of laser magnetic field when laser intensity is 10^{19} W/cm^2 and is comparable to the PIC prediction [4]. The electrostatic field at the rear side of the target [11,12] is another possibility to bent the electrons to the target surface direction. The static field, $E \sim kT_H/el_D$, where T_H is the electron temperature and l_D the Debye length, is directed toward the target normal direction and affects within the Debye length. From the electron temperature calculated above, the static field and Debye length in our case must be order of 10^{12} V/m and microns. However, the strength of the static field required to distort the electron emission direction is just order of 10^{10} V/m. Moreover, if the change of emission angle is due to the electrostatic field, it is extremely difficult to explain the difference of emission angle with and without plasma conditions. From these considerations, the surface magnetic field is most likely to be formed only when the laser intensity is sufficiently high and the plasma scale length is less than a micron. In our case, these conditions could be achieved by increase of laser intensity due to relativistic self-focusing[13].

3 Hot electron generation with low density foam for fast ignition

The energy coupling from the relativistic laser into the compressed core plasma is one of the most important key issues in the FI. With the gold cone-in-shell target design for the FI, the relativistic laser is focused on the inner tip of the solid density gold cone to generate hot electrons. The electrons then transport into the core plasma and deposit their energy there for heating. Increasing the energy conversion efficiency from the laser into hot electrons will enhance the heating of the core plasma. Several processes such as vacuum heating and ponderomotive J×B acceleration are responsible for the hot electron generation in the relativistic laser interaction with the solid target [14]. Energy coupling efficiency up to 40% from 0.1 PW laser to the hot electrons has been demonstrated [15]. The energy conversion efficiency from the laser into hot electrons with solid targets may be enhanced through increasing the laser intensity [16].

However, increasing the laser intensity will simultaneously increase the hot electron temperature with solid targets, resulting in the reduction of the hot electron energy deposition efficiency into the core plasma. The hot electron energy deposition efficiency is strongly dependent on the hot electron temperature. The hot electrons with low temperature are beneficial for their energy deposition since the stopping power of hot electrons in the core plasma increases when the electron temperature softens. Integrated experiments with gold cone-in-shell targets have showed that 30% of 0.1 PW laser energy can be coupled into the imploded core plasma, while the coupling efficiency is reduced down to ~20% for 0.5 PW laser [17]. The reduction of the laser energy coupling efficiency was attributed to the increase of the hot electron temperature when the laser power was increased. At ignition level, several 10 kJ laser energy is required and must be delivered within the disassembly time duration (several 10 ps) of fuel core plasma, resulting in a relativistic laser power equivalent to 1 PW or higher. At 1 PW, the laser energy coupling efficiency would be further reduced as the temperature of hot electrons becomes even higher. Finally unreasonably large PW laser energy will be required to reach ignition conditions.

Methods to increase the UIL absorption and hot electron energy conversion efficiency without increasing the hot electron temperature are therefore of great interest for the FI. We here propose to utilize metal or plastic foams for these purposes. The foam has a local solid density with a low average density. Our proposed foam cone-in-shell target design for the FI is based upon the gold cone-in-shell target design [18] and schematically shown in Fig.4. The inner tip of a solid gold cone is covered with a thin low-density foam layer. The

relativistic laser is focused on the foam instead of the solid cone tip to generate hot electrons for the FI. Element physics experiments demonstrate enhanced hot electron production without increasing the hot electron temperature from planar solid targets with thin low-density foam coating on the front surface, indicating that our proposed foam cone-in-shell target has advantages over the gold cone-in-shell target successfully used for the FI.

Figure 4 Proposed foam cone-in-shell target design for the fast ignition, showing the relativistic laser irradiates the thin low-density metal or plastic foam layer which covers the inner tip of a solid gold cone inserted in a fuel shell.

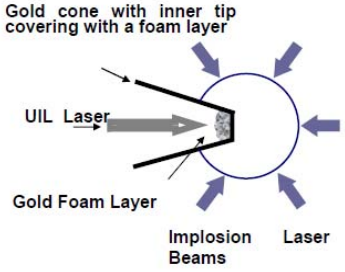

To examine the feasibility of our proposed foam cone-in-shell target design for the FI, we performed element physics experiments on both GXII PW laser and GMII laser at the Institute of Laser Engineering, Osaka University. Both GXII PW and GMII lasers have a very high contrast ratio against a prepulse with optical parametric chirped pulse amplification as the front end. The pulse duration of both lasers after compression was about 0.6 ps. The maximum output energies on targets were about 450 and 10 J, with the focus spot sizes of about 70 and 25 μm, respectively for the GXII PW and GMII lasers. The p-polarized GXII PW laser and GMII laser irradiated the targets at 26^0 and 20^0 to the target normal, respectively. The targets used were planar solid foils with front surface coating with low-density gold foams, resembling the gold cone inner tip covered with the low-density foam, as shown in Fig.1. Planar solid targets without foam coating on the front surface were used as the reference. Investigations were focused on the laser energy conversion efficiency into hot electrons, the hot electron temperature and angular distribution.

Figure 5 shows the keV x-ray pinhole camera (XPHC) images taken from both front and back of the targets irradiated by the GXII PW laser. The targets used were 20 μm thick molybdenum with front surface (i.e., laser interaction side) coated by either 2 μm solid gold or 2 μm gold foam. The laser energy was 100 J with a 0.6 psec pulse width. The density and porous cell size of the gold foam were 20% of the solid gold and about 0.3 μm [19]. The front XPHC monitored the laser interaction dynamics and had a 18 μm small pinhole with 40 μm thick beryllium filter. The rear XPHC monitored the heating of the rear surface of the target and had a 200 μm large pinhole with 40 μm thick beryllium filter. Thus both XPHCs had the x-ray spectral sensitivity in the range 1-30 keV, with an effective peak of the spectral response at about 5 keV. The front x-ray emission from the gold foam coating target is weaker than the solid gold coating target. However, the rear x-ray emission from the gold foam coating target is much stronger than the solid gold coating target. The total count of the rear x-ray emission intensity from the gold foam coating target is about *3 times* of the solid gold coating target. The rear x-ray emission intensity reflects the deposited energy density located at the rear surface of the target and the heating of rear surface of the target. Higher x-ray emission count implies larger energy deposited. The deposited energy and heating are mainly from the hot electrons [20] generated at the front of the target during the laser interaction. These hot electrons transport through the bulk target to heat the rear surface, resulting in the rear x-ray emission. Note the x-rays generated from the laser interactions at front surfaces cannot be responsible for the enhancement of the rear x-ray emission from the gold foam coating target. The target is too thick for keV x-rays to transmit from the front to the rear of the target. Moreover, with gold foam coating target the x-ray emission from the target front is weaker, thus one would expect a weaker rear x-ray emission, contrary to the experimental result, due to the x-ray transmission from the target front. We thus conclude that with the gold foam coating on the front surface, more laser energy is absorbed and coupled

into hot electrons, resulting in the enhancement of both heating of the rear surface of the target and rear x-ray emission.
We should point out that the GXII PW laser energy was only 15% larger but the rear x-ray emission was about 2 times stronger in the gold foam coating target case. We consider that the enhanced rear x-ray emission is not due to larger laser energy but to enhanced laser energy absorption and hot electron production in the laser-foam interaction.

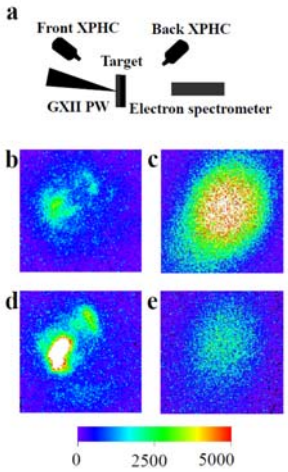

Figure 5. (Color) x-ray pinhole camera (XPHC) images taken from the front and rear of the targets. (a) is the experimental setup. (b) and (c) are the front and rear XPHC images from the solid gold coating target, (d) and (e) are the front and rear XPHC images from the gold foam coating target, respectively. The front x-ray emission is weaker while the rear x-ray emission is stronger from the gold foam coating target in comparison with the solid gold coating target. The rear x-ray emission is due to the heating of rear surface of the target by hot electrons generated in the GXII PW laser interactions. The GXII PW laser energies were 113 J and 98 J for gold foam and solid gold coating targets, respectively.

The hot electron spectra were measured with an electron spectrometer placed behind the targets along the GXII PW laser axis. The spectrometer is equipped with a pair of magnets with a field strength of 4.5 kG. The hot electron spectra are very similar for 2 μm solid gold coating and 2 μm gold foam coating targets, showing a temperature ~1.5 MeV, a typical value for solid plastic or aluminum targets. We attribute the enhanced hot electron production from the gold foam coating target, as evidenced by the x-ray emissions shown in Fig.2, to the micro-structure of the foam. Structuring the target surface reduces the laser reflectivity and significantly increase the laser absorption [21-24]. It has been shown that the micro-structured targets, such as gratings and gold black [21], "velvet" coatings [22], porous and nanocylinder [23], and metal nanoparticle coatings [15], are more efficient at absorbing the intense laser energy than the polished solid targets. As a result, significant enhancements have been demonstrated in emissions of soft x-rays [21-23], and hard x-rays [24] which is a signature of hot electrons created in the laser interactions. Enhanced hard x-ray yield implies enhanced hot electron production. Specifically, a porous cell of the gold foam behaves as a hohlraum to the laser light, increasing laser energy coupling into hot electrons. The use of a low-density foam layer covering the solid gold cone tip, as shown in Fig.4, can be thus expected to facilitate highly efficient conversion of the laser into hot electrons simultaneously without increasing the hot electron temperature for the FI[25].

4. Summary

We observed spatial distributions of fast electrons emitted in intense laserp lasma interactions. The emission angle changed from the specular direction to the target surface direction when preformed plasma is presented in front of the solid target. In addition, the emission angle also becomes close to target surface with increasing laser intensity. This change could be caused by formation of strong static magnetic field along the target surface due to trapping of fast electron at the surface. The relativistic self-focusing in our plasma condition gives the higher laser pressure which is significantly required for the surface current formation. The strength of magnetic field is calculated from the bending angle of the emitted electrons detected each layer of detector, resulting in order of 10% of laser magnetic field. Such strong electron current along with surface might bring the high

conversion efficiency on the cone-guided fast ignitor experiments. We proposed a novel foam cone-in-shell target design for the FI. Elementary physics experimental result show that the laser energy coupling efficiency into the hot electrons can be enhanced without increasing the electron temperature by use of low-density foam, indicating the proposed target design has advantages over the gold cone-in-shell target ever used and promising for the FI. The experimental result indicate by optimizing the thickness and density of the foam, it might be possible to reduce the hot electron temperature.

Acknowledgement

We all thank the hard work supported by the laser, target, and technical groups at ILE, Osaka University. A.L.L and G.R.K are supported by the visiting scholar system of JSPS at the Osaka University. A.L.L. also acknowledges the Core University Exchange program organized by the National Institute of Fusion Science under JSPS.

Reference

[1] P. A. Norreys et al., Phys. Plasmas **7**, 3721 (2000) ; R.Kodama et al., Nature **418** (2002) 233; K.A. Tanaka et al., Phys. Plasmas **10** (2003) 1925.
[2] Y. Sentoku et al., Phys. Plasmas **11** (2004) 3183; T. Nakamura et al., Phys Rev. Lett. **93** (2004) 265002.
[3] R. Kodama et al., Nature **412**, 798 (2001).
[4] Y. Sentoku, K. Mima, H. Ruhl, Y. Toyama, R. Kodama, and T.E. Cowan, Phys. Plasmas **11**, 3083 (2004); T. Nakamura, S. Kato, H. Nagatomo, and K. Mima, Phys. Rev. Lett. **93**, 265002 (2004).
[5] Y. Kitagawa et al., Fusion Engineering and Design **44**, 261(1999).
[18] H. Takabe et al., Phys. Fluids **31**, 2884 (1988).
[6] K. A. Tanaka, T. Yabuuchi, T. Sato, R. Kodama, Y. Kitagawa, T. Ikeda, Y. Honda, and S. Okuda, Rev. Sci. Instrum. **76**, 013507 (2005).
[7] R. Kodama, K. A. Tanaka, Y. Sentoku, T. Matsushita, K. Takahashi, H. Fujita, Y. Kitagawa, Y. Kato, T. Yamanaka, and K. Mima, Phys. Rev. Lett. **84**, 674 (2000).
[8] C. Gahn et al., Phys. Plasmas **9**, 987 (2002).
[9] Y. T. Li et al., Phys. Rev. E **69**, 036405 (2004).
[10] E. Lefebvre and G. Bonnaud, Phys. Rev. Lett. **74**, 2002 (1995).
[11] S. P. Hatchett et al., Phys. Plasmas **7**, 2076 (2000).
[12] R. A. Snavely et al., Phys. Rev. Lett. **85**, 002945 (2001).
[13]H. Habara, K. Adumi, K.A. Tanaka et al., To appear in Phys. Rev. Lett. (2006).
[14] F. Brunel, Phys. Rev. Lett. **59**, 52 (1987); G. Malka *et al.,* Phys. Rev. Lett. **79**, 2053 (1997); Y. Sentoku *et al.,* Phys. Plasmas **11**, 3083 (2004).
[15] R. Kodama *et al.,* Phys. Plasmas **8**, 2268 (2001).
[16] M. H. Key *et al.,* Phys. Plasmas **5**, 1966 (1998).
[17]R. Kodama *et al.,* Nature **412**, 798 (2001).
[18] R. Kodama *et al.,* Nature **418**, 933 (2002).
[19] K. Nagai *et al.*, Fusion Sci. Technol., in press.
[20] E. Martinolli *et al.*, Phys. Rev. E **70**, 055402(R) (2004).
[21] M.M. Murnane *et al.*, Appl. Phys. Lett. **62**, 1068 (1993).
[22] G. Kulscár *et al.*, Phys. Rev. Lett. **84**, 5149 (2000).
[23] T. Nishikawa *et al.*, Appl. Phys. Lett. **70**, 1653 (1997); T. Nishikawa *et al.*, Appl. Phys. Lett. **75**, 4079 (1999).
[24] P. P. Rajeev *et al.*, Phys. Rev. Lett. **90**, 115002 (2003).
[25] A.L. Lei, K.A. Tanaka et al., Phys. Rev. Lett, **96**, 255006 (2006).